

Radiative effects of black carbon aerosols on Indian monsoon: a study using WRF-Chem model

Pramod Soni¹  · Sachchida Nand Tripathi¹ · Rajesh Srivastava¹

Received: 27 January 2016 / Accepted: 19 January 2017
© Springer-Verlag Wien 2017

Abstract The Weather Research and Forecasting model with Chemistry (WRF-Chem) is utilized to examine the radiative effects of black carbon (BC) aerosols on the Indian monsoon, for the year 2010. Five ensemble simulations with different initial conditions (1st to 5th December, 2009) were performed and simulation results between 1st January, 2010 to 31st December, 2010 were used for analysis. Most of the BC which stays near the surface during the pre-monsoon season gets transported to higher altitudes with the northward migration of the Inter Tropical Convergence Zone (ITCZ) during the monsoon season. In both the seasons, strong negative SW anomalies are present at the surface along with positive anomalies in the atmosphere, which results in the surface cooling and lower tropospheric heating, respectively. During the pre-monsoon season, lower troposphere heating causes increased convection and enhanced meridional wind circulation, bringing moist air from Indian Ocean and Bay of Bengal to the North-East India, leading to increased rainfall there. However, during the monsoon season, along with cooling over the land regions, a warming over the Bay of Bengal is simulated. This differential heating results in an increased westerly moisture flux anomaly over central India, leading to increased rainfall over northern parts of India but decreased rainfall over southern parts. Decreased rainfall over southern India is also substantiated

by the presence of increased evaporation over Bay of Bengal and decrease over land regions.

1 Introduction

Black carbon (BC) aerosols are the strongest light absorbing tiny (0.1 to 1 μm) particles formed due to inefficient burning of fossil fuels, bio-fuels and bio-mass (Collins et al. 2002). BC in soot particles is the second-most important contributor to the observed twentieth century global warming after CO_2 (Jacobson 2002). Absorbing aerosols (BC, organic carbon, dust etc.) primarily influence the solar radiation budget by absorbing radiation at all wavelengths causing strong atmospheric heating in the troposphere. On the other hand, scattering aerosols (seas salts, sulphates, nitrates, etc.) scatter the radiation. Both types of interactions lead to cooling at the surface, and this phenomenon is commonly called direct effect of aerosols (Meywerk and Ramanathan 1999). By acting as cloud condensation nuclei (CCN) or ice nuclei (IN), most of the aerosols in the atmosphere participate in the cloud microphysical processes, leading to changes in cloud number concentration, particle size, and radiative properties; which is commonly known as the indirect effect of aerosols (Twomey 1977). The atmospheric heating induced by absorbing aerosols can lead to evaporation of clouds droplets and changes in cloud optical depths, known as semi-direct effect (Hansen et al. 1997; Ackerman et al. 2000; Kaufman and Koren 2006).

Indian subcontinent is one of the most heavily industrialized and densely populated regions of the world, hence aerosols in this region can potentially affect global climate (Ramanathan and Carmichael 2008). Many observational studies have reported high aerosol concentrations over various Indian cities (Babu et al. 2013; Ganguly et al. 2006;

✉ Pramod Soni
pramods@iitk.ac.in

Sachchida Nand Tripathi
snt@iitk.ac.in

Rajesh Srivastava
rajeshs@iitk.ac.in

¹ Indian Institute of Technology, Kanpur, 208016, India

Ramachandran and Cherian 2008; Safai et al. 2007; Pervez et al. 2016). Majority of aerosols over Indo-Gangetic-Plains (IGP) are predominantly of absorbing type, thus IGP has been recognized as a regional BC hotspot (Ramanathan and Ramana 2005; Niranjana et al. 2007; Prasad and Singh 2007; Gautam et al. 2011; Giles et al. 2011; Srivastava et al. 2012). Since 70–80% of energy requirement in rural India is still met by traditional bio-fuels combustion, about 80% of emitted carbonaceous aerosols in India are originated from the use of biomass for energy (Parashar et al. 2005). BC emissions in India have increased from 0.72 Tg in 1996 to 1.02 Tg in 2010 (about 2.5% annual growth rate), with bio-fuel (45–52%), coal (22–29%), and oil (14–17%) being the dominant contributors (Lu et al. 2011).

The Indian Ocean Experiment (INDOEX) was an international, multi-platform field campaign to measure long-range transport of air pollution from South and Southeast Asia toward the Indian Ocean during the dry monsoon season from January to March 1999. High pollution levels were observed over the entire northern Indian Ocean toward the ITCZ at about 6°S (Lelieveld et al. 2001). Using data from INDOEX experiment, Ramanathan et al. (2001) found that BC contributed about 14% to the fine particle mass in Indo-Asian haze, commonly known as Atmospheric Brown Clouds (ABC), and had a single-scattering albedo of around 0.9 over south Asia.

Numerous modeling studies to investigate ABC effects have been conducted with Global Climate Models (GCM) with fixed sea surface temperatures (SST). Chung et al. (2002) performed climate scale simulations during November–May and analyzed ABC effects over South Asia and found a significant increase of rainfall there. Long-term drought over northern China and excessive rainfall over southern China were attributed to changes in atmospheric circulation induced by BC (Menon et al. 2002). Elevated heat pump (EHP) hypothesis was proposed by Lau et al. (2006), which states that dust and BC induced heating can enhance the monsoon rainfall over northern parts of India through large-scale dynamical feedback.

Decreased rainfall via reduction in meridional SST gradient induced by ABC were simulated using coupled atmosphere-ocean models Ramanathan et al. (2005) and Chung and Ramanathan (2006). By conducting ensemble simulations with a similar model, Meehl et al. (2008) showed that BC can have different effects on rainfall during monsoon and pre-monsoons seasons. Wang et al. (2009) showed that anthropogenic absorbing aerosols can cause heavy rainfall over North-West India by altering the meridional gradient of the moist static energy. Observed decrease in precipitation during monsoon season over IGP was attributed to increasing anthropogenic aerosols (Bollasina et al. 2011). Ganguly et al. (2012b) reported that feedback

associated with SST change (slow response) due to anthropogenic aerosols play a more important role than the direct impact (fast response) of the aerosols on radiation, clouds and land surface.

A key limitation of GCMs is the fairly coarse horizontal resolution which cannot accurately represent sub-grid level processes (moist convection, diffusion, clouds, etc.) and properties (vegetation, coastlines, and uneven terrain). Regional climate models (RCM) with fine resolution can simulate these features more accurately. Very few modeling studies on this subject have been conducted with fine resolution regional models.

Using the regional climate model (RegCM) version 4.1, a positive feedback of the aerosol direct radiative forcing on the summer monsoon circulation over India was found through dynamical changes (Das et al. 2015a). The large-scale convergence induced by dust aerosols over the Arabian Peninsula plays an important role in strengthening the monsoon circulation leading to enhanced precipitation over India (Das et al. 2015b). Observed increasing summer precipitation over southern India during 2000–2009 was attributed to increasing Arabian dust emissions (Solomon et al. 2015). Das et al. (2016) also used RegCM4.1 and analyzed the direct radiative impacts of all anthropogenic aerosols on the dynamics of Indian summer monsoon circulation and found that aerosol-induced cooling is responsible for the weakening of summer monsoon circulation over India.

In an observational study by Bollasina et al. (2008), it was reported that absorbing aerosols can reduce cloud cover over India via semi-direct effect, leading to reduced precipitation, increased SW radiation and thus heating at the surface. By analyzing active and break monsoon periods using satellite data, Manoj et al. (2011) showed that absorbing aerosol loading over Indian region during monsoonal break period can facilitate the transition of Indian summer monsoon breaks to active spells, and therefore increase the rainfall. Analyzing satellite data from Moderate Resolution Imaging Spectroradiometer (MODIS) and Global Precipitation Climatology Project (GPCP), along with numerical simulations, Vinoj et al. (2014) found a positive correlation between dust aerosol over the Arabian Sea (AS) and the amount of rainfall over central India during the monsoon season.

So far, effects of only BC aerosols have not been analyzed using a high-resolution regional climate model. All the modeling studies analyzing BC radiative effects on Indian monsoon have been performed with coarse resolution GCM and non-interactive aerosols forcing. The response of the Indian monsoon to aerosol depends on the way the aerosols are treated in the model and reliability of the model to simulate the observed monsoon climate. Since BC is the most absorbing type of aerosol in atmosphere, there is a

need to assess its effects at regional level using a high resolution RCM. A high resolution, fully chemistry coupled, regional climate model, with interactive aerosol scheme could simulate such regional effects more accurately. The Weather Research and Forecasting model with Chemistry (WRF-Chem) (Grell et al. 2005) has the option to simulate the coupling between dynamics, radiation, and chemistry. It simulates the emission, transport, mixing, and chemical transformation of trace gases and aerosols simultaneously with the meteorology to give more accurate representation of aerosols in the atmosphere. The main objectives of this study are -

1. Evaluation of WRF-Chem model for simulating meteorological variables over India.
2. To understand how BC aerosols effect radiation directly.
3. To analyze thermodynamic and meteorological changes by virtue of radiation anomalies induced by BC aerosols.
4. To analyze the effect of changing dynamics on precipitation over India.

Brief description of the model along with experimental setup is provided in Section 2. For model evaluation, a comparison of simulated meteorological variables (rainfall, winds, aerosol optical depth, BC concentration, and temperature) with the observational and satellite data is given in Section 3. Direct effects of BC aerosols on clouds, SW heating rate, radiation, temperature, winds, and thus rainfall are discussed in Section 4. Summary and conclusion are provided in Section 5.

2 Model description and experimental setup

Five ensemble simulations were performed using WRF-Chem version 3.4.1 with the model domain covering entire India, centered at 22 degree N, 80 degree E and having 139×137 grid points at 30 km horizontal resolution as shown in Fig. 1. Year 2010 was chosen based on the availability of observational data and it being a normal monsoon year (IMD 2010). Two sets of experiments were performed, one with all aerosol emissions present (referred to as CTRL) and other without BC emissions (referred to as NOBC). A total of five ensemble simulations for each set were conducted by shifting the initial conditions by one day from 1st December 2009 to 5th December 2009. Simulation results from 1st January, 2010 to 31st December, 2010 were analyzed, considering initial 1-month period as spin up time of the model.

Table 1 lists all the model parameters used in this study. Removal of aerosols by wet scavenging is an important process to be considered in the model, ignoring which can lead to overestimation of the aerosols. To include this process but to exclude CCN activities (for ignoring indirect effects),

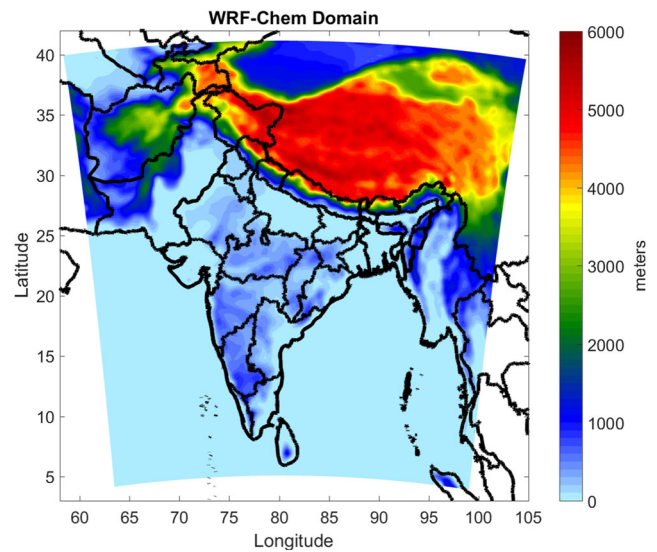


Fig. 1 WRF-Chem domain with topography

aerosol CCN processes were disabled by turning off the ‘mixactivate’ routine (responsible for CCN activation) in the model.

3 Model evaluation

3.1 Rainfall and winds

The simulation of surface precipitation in large-scale atmospheric models is essentially the end product of a long line of various parameterization schemes. All parameterization schemes have inherent uncertainties which ultimately project onto the simulated rainfall—which is, of course, the prime reason why models generally struggle to adequately simulate surface rainfall, especially over low latitudes (Randall et al. 2007; Flato et al. 2013). Figure 2a, b shows observed (Tropical Rainfall Measuring Mission, TRMM 3B42) and simulated (CTRL) zonal mean (65E-95E) precipitation for year 2010, respectively. Stippling in the Fig. 2b indicate grids where ensemble mean divided by standard deviation exceeds 1. Indian monsoon slowly sweeps across the country beginning in early June and recedes from North India in the beginning of October with south and northeast India typically receiving more rainfall.

Spatial features of the Indian monsoon are simulated fairly well by the model, with some over-estimation near 10 N, which are mostly oceanic regions. Figure 2c shows all India average monthly time series from TRMM, Indian Meteorological Department (Pai et al. 2014), Climate Research Unit (CRU) (Harris et al. 2014), and CTRL

Table 1 Model configuration

Model parameter	
Number of grid points	139 × 137 × 27
Horizontal grid projection	Lambert conformal
Horizontal resolution	30 km × 30 km
Vertical grid	Stretched grid with about 11 levels in boundary layer
Model top	50 hPa
Model domain center	22° N, 80° E
Initial and boundary conditions	NCEP FNL reanalysis (http://rda.ucar.edu/datasets/ds083.2/)
Anthropogenic emissions	Global emissions (Schultz et al. 2007) Local emissions (Venkataraman et al. 2006)
Dust parameterization	MADE/SORGAM (Ackermann et al. 1998; Schell et al. 2001)
chemical mechanism	RADM2 (Stockwell et al. 1990)
aerosol module	MADE/SORGAM (Ackermann et al. 1998; Schell et al. 2001)
SW and LW radiation	RRTMG (Iacono et al. 2008)
Microphysics	Morrison double moment (Morrison et al. 2009)
Cumulus parameterization	NSAS (Han and Pan 2011)

simulation. Ensemble spread of the model is shown by multiple dashed blue lines, one for each ensemble. Model shows good agreement with all the observations.

Scatter plot of all India average cumulative rainfall for year 2010 between TRMM and CTRL simulation

(corresponding to the observed grid, closest matching model points were chosen from a spatial window of 90 km) is plotted in Fig. 2d which gives a relative root mean squared error (RRMSE) of about 27% and R^2 of 0.8. These performance statistics indicate adequate performance of model in terms

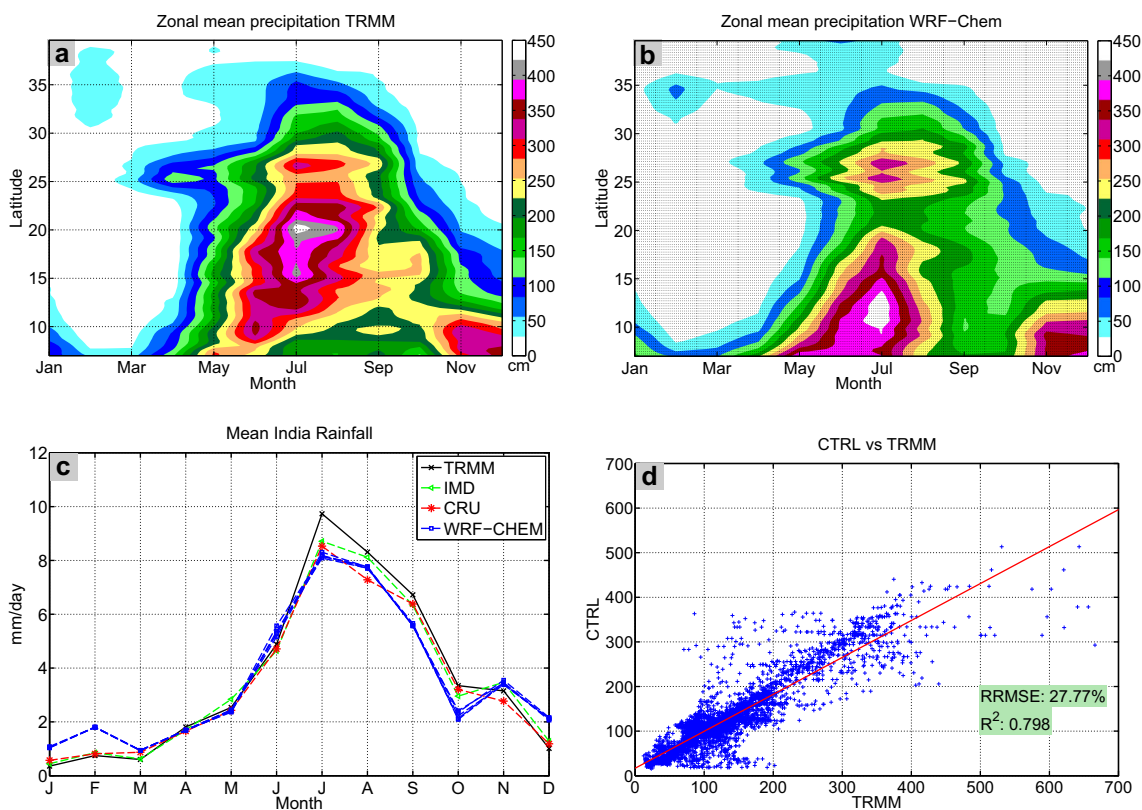


Fig. 2 Monthly zonal mean precipitation **a** TRMM and **b** Model (Stippling indicates areas, where ensemble mean divided by ensemble standard deviation exceeds 1). **c** Mean India monthly time series

precipitation (spread of ensembles is shown with multiple *dashed blue lines*, one for each ensemble). **d** Scatter plot of yearly cumulative rainfall over India

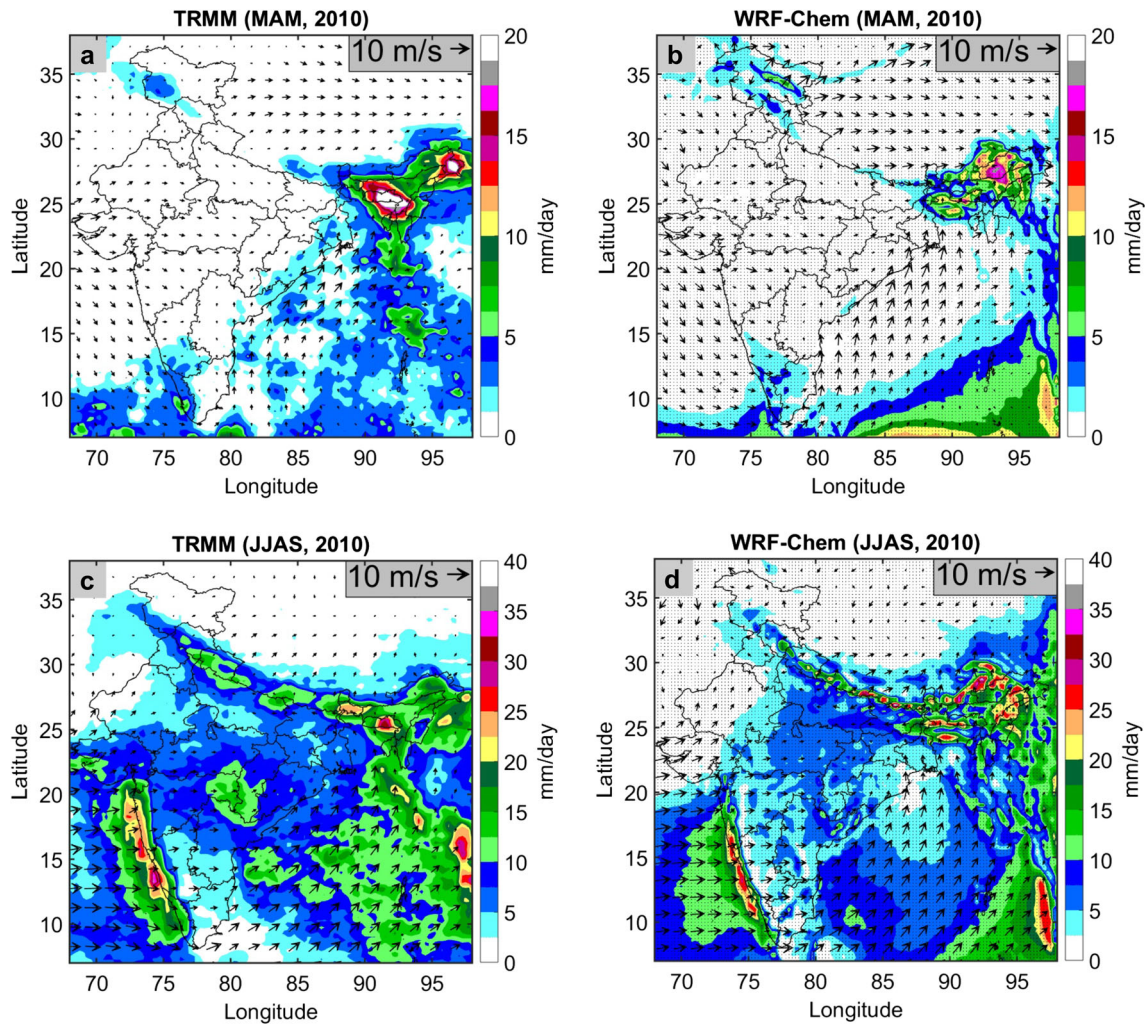


Fig. 3 Mean precipitation rate (mm/day) and 10 m wind vector (m/s) **a** and **c** TRMM and ERA-Interim for JJAS and MAM, respectively, **b** and **d** WRF-Chem. Stippling in **b** and **d** indicate areas, where ensemble mean divided by ensemble standard deviation exceeds 1

of mean and cumulative precipitation over India. Although there are some spatial differences between the model and observed rainfall, prominent features of Indian monsoon are simulated quite satisfactorily by the model.

Figure 3a, c shows the spatial pattern of cumulative precipitation from TRMM along with 10 m horizontal wind vectors from European Centre for Medium-Range Weather Forecasts Re-Analysis (ERA)-Interim reanalysis data (<http://dss.ucar.edu/datasets/ds627.0/>) (Dee et al. 2011) for monsoon (June–July–August–September, referred to as JJAS) and pre-monsoon (March–April–May, referred to as MAM) seasons, respectively. Similar plots are drawn for CTRL simulation in Fig. 3b, d. Stippling indicate grids where ensemble mean divided by standard deviation exceeds 1.

During the pre-monsoon season, south-westerly winds cause precipitation over northeast India by drawing moist

air from Bay of Bengal and Indian Ocean. However, along with the westerly jet from Arabian Sea, these winds cause heavy rainfall over entire India during the monsoon season. Model is able to simulate spatial features of rainfall and winds accurately. Heavy rainfall over western-Ghats and northeast India during the monsoon season is adequately captured by the model, but over the Bay of Bengal, rainfall is significantly underestimated during both the seasons. Overall, spatial features of winds and rainfall associated with the Indian monsoon are simulated reasonably well. Tropical atmospheres have a unique and fundamental property, that large-scale seasonal circulation and rainfall are almost completely determined by the boundary conditions of SST (Shukla 1998). Large-scale circulation and SST forced forced at the lateral boundaries of the model domain could be the reasons for the model simulating the circulation accurately.

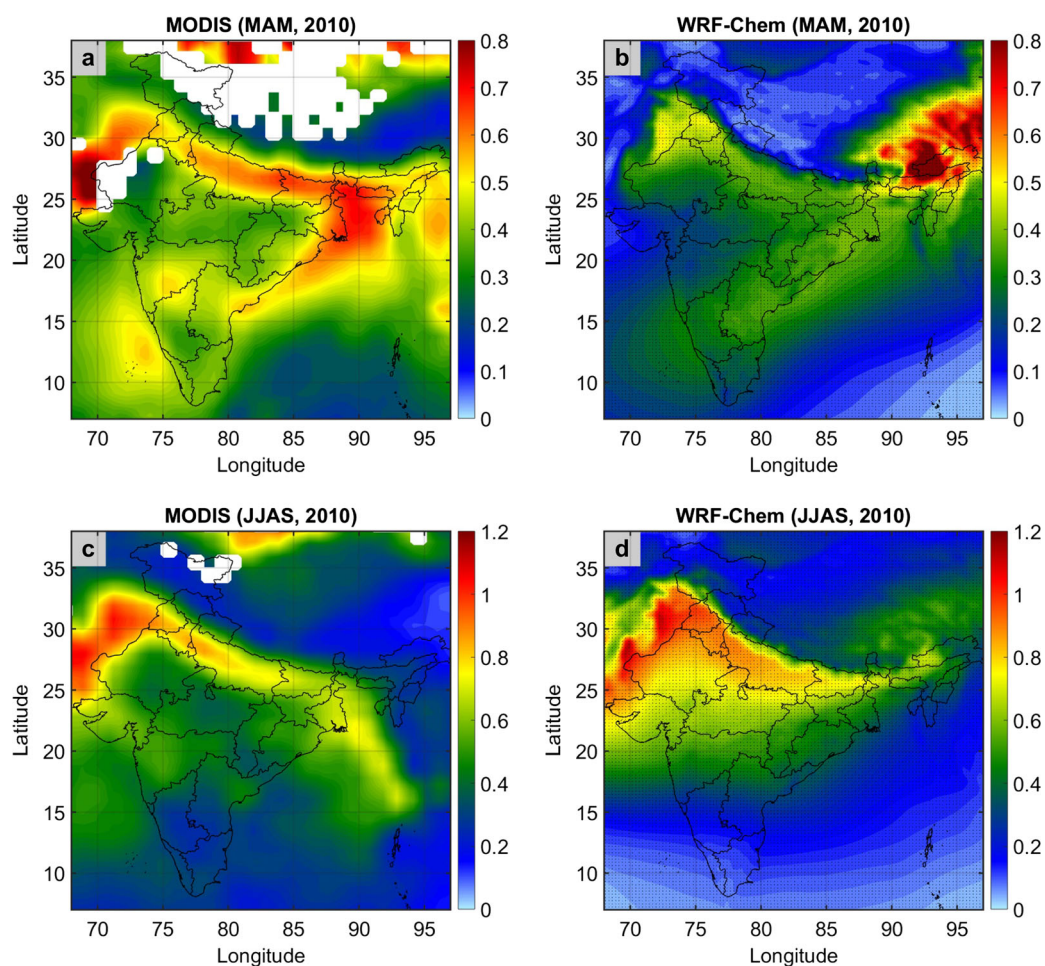


Fig. 4 AOD from MODIS and WRF-Chem. Stippling indicates areas where ensemble mean divided by ensemble standard deviation exceeds 1

3.2 Aerosol optical depth and BC surface concentration

Aerosol optical depth (AOD) at 550 nm from MODIS (Remer et al. 2005) and CTRL simulation during monsoon and pre-monsoon season are shown in Fig. 4. There is about 50% underestimation in AOD by the model compared to MODIS, especially during the pre-monsoon season. However, during the monsoon season, a slight overestimation is noted over the IGP. Underestimation of AOD is not uncommon in models (Menon et al. 2010; Wu et al. 2013; Ganguly et al. 2012a; Henriksson et al. 2011), which can be due to lower values of anthropogenic emission factors or due to poor parameterization of dust (it is the major contributor to the AOD over IGP). In spite of that, the model is able to capture spatial features of AOD fairly well.

Simulated AOD is also evaluated at four Aerosol Robotic Network (Aeronet) (Holben et al. 1998) stations. Data from Multiangle Imaging Spectroradiometer (MISR), MODIS and Aeronet AOD at Jaipur (26.9 N, 75.80 E), Kanpur (26.51 N, 80.23 E), Nainital (29.35 N, 79.45 E) and Gandhi College (25.87 N, 84.12 E) are plotted with simulated AOD

on weekly timescale in Fig. 5. During the pre-monsoon season, the model underestimates AOD, whereas during the monsoon season it matches closely with the observations.

Surface observations of BC concentration, measured using an aethalometer, were available from March, 2010 to June, 2010 at Indian Institute of Technology (IIT), Kanpur. Figure 6 shows the weekly time series of simulated and measured BC surface concentration at IIT Kanpur. Simulated BC concentration is in good agreement with the measurements, and lies within the range of 5–10 g/kg.

3.3 Temperature

Surface temperature data from automatic weather stations (AWS) was used to compare with simulated surface temperature. Mean India time series of surface temperature from 298 AWS stations and CTRL simulation is shown in Fig. 7a. Model temperature time series consistently agrees with observations. Scatter plot between the AWS and simulated daily surface temperature is also shown in Fig. 7b, with an RRMSE of about 6.62% and R^2 of 0.8.

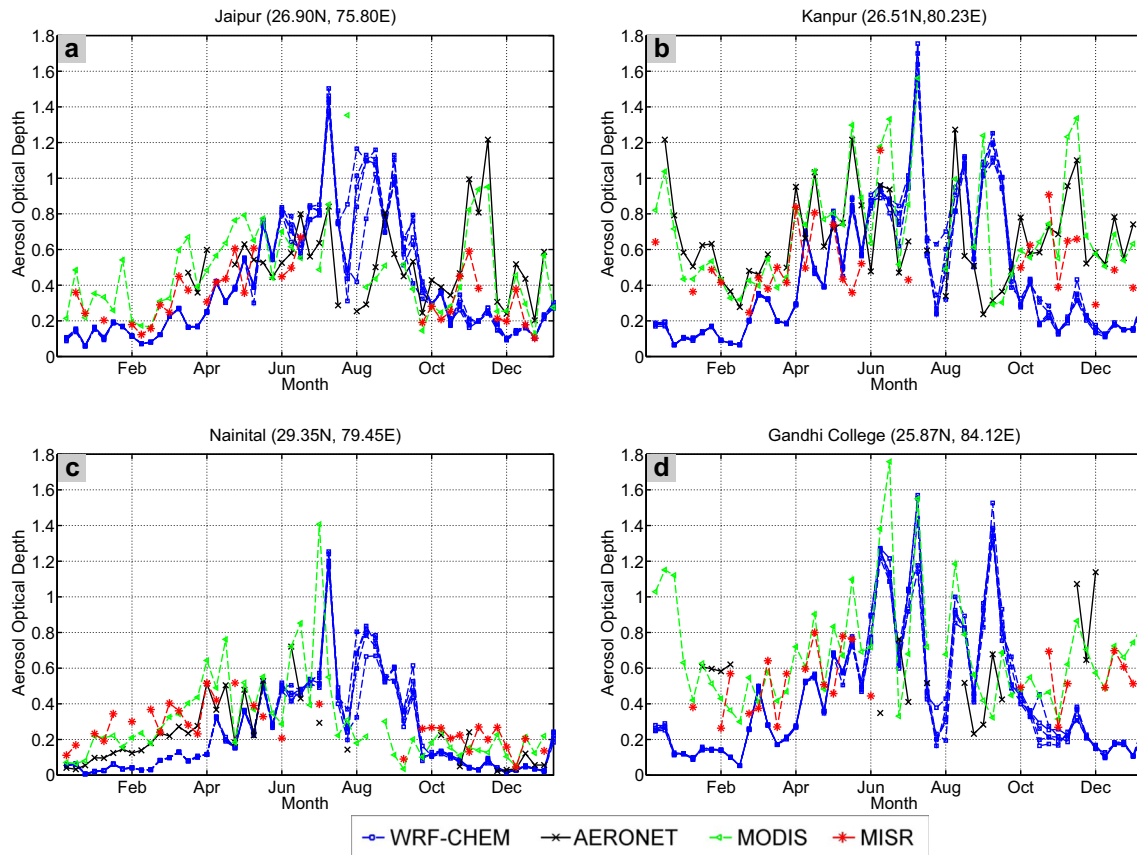


Fig. 5 Weekly AOD from observations and model at four AERONET stations **a** Jaipur, **b** Kanpur, **c** Nainital, and **d** Gandhi College. (spread of ensembles is shown with multiple blue lines, one for each ensemble)

4 Radiative effects of BC aerosols

The model setup, as used in this study, allows for quantifying only the direct and semi-direct radiative effects of the anthropogenic aerosols. Hence, by subtracting NOBC

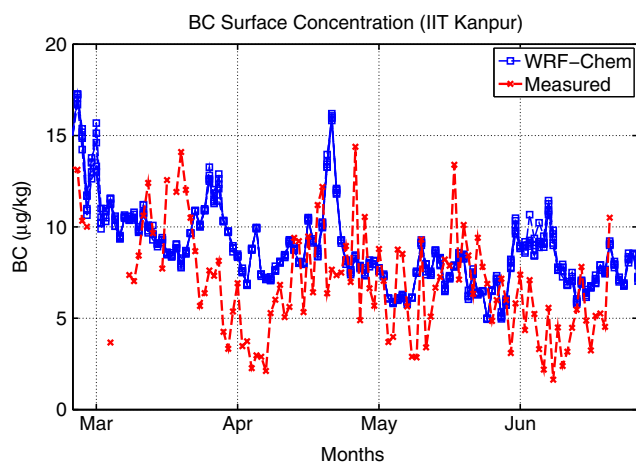


Fig. 6 BC surface concentration at IIT Kanpur (spread of ensembles is shown with multiple blue lines, one for each ensemble)

simulation from CTRL simulation, radiative effects of BC aerosols can be assessed. Effects of BC aerosols on various meteorological variables and including precipitation are discussed in this section.

4.1 Distribution of clouds, BC aerosols, and shortwave heating

Anomalies of BC concentration ($\mu\text{g}/\text{kg}$), SW heating rate (K/day) and cloud fraction (%) calculated from CTRL – NOBC are shown in Fig. 8. Sub-figures (a), (d), and (g) show zonal mean (70E–100E) anomalies during the pre-monsoon season, whereas (b), (e), and (h) show similar plots during the monsoon season for these variables. Mean vertical profiles of these variables over different regions and seasons are shown in sub-figures (c), (f), and (i). It can be seen from sub-figures (a), (b), and (c) that most of the BC which is located below 6 km during the pre-monsoon season is transported to higher altitudes in the monsoon season, which is due to the advancement of ITCZ over India during monsoon season. High BC concentration ($3 \mu\text{g}/\text{kg}$) is simulated near surface, over the land regions, which reduces with altitude and concentration is negligible above 8 km

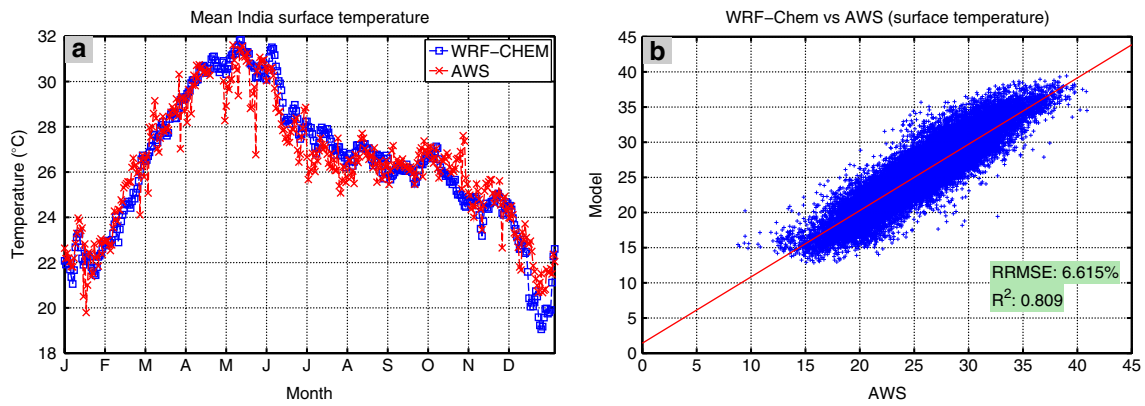


Fig. 7 a Mean India surface temperature. b Scatter plot of daily surface temperature from WRF-Chem and AWS stations (all units are in °C)

(sub-figure (c)). Since BC is highly absorbing in nature, SW radiative heating rate shows pattern similar to BC concentration (sub-figures (c) and (f)). Increased elevated SW heating

rate above 8 km can be seen during the monsoon season as compared to pre-monsoon season (sub-figure (f)). Due to increased near surface heating, increased cloud fraction

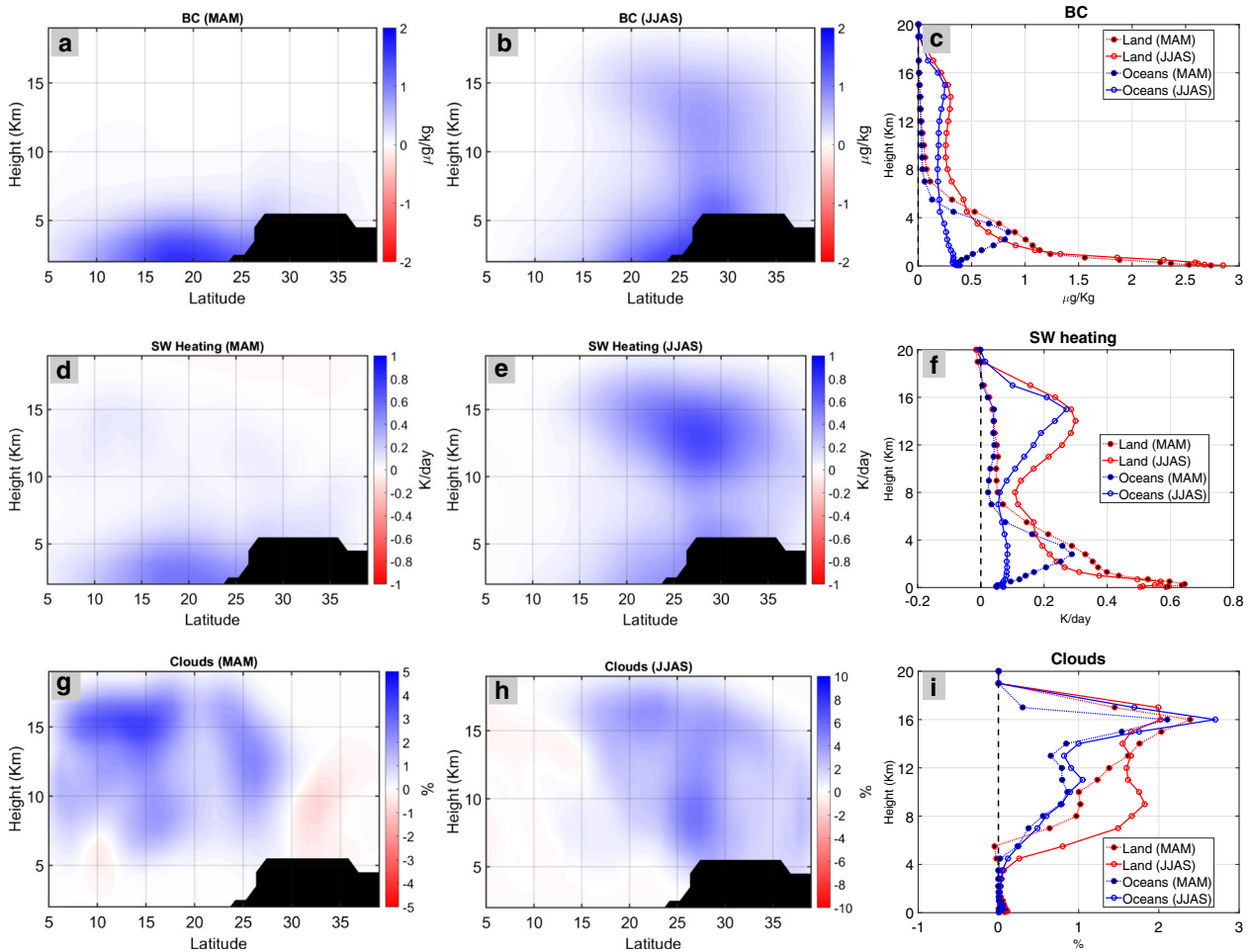


Fig. 8 Sub-figures (a), (d), and (g) show zonally averaged (70–100E) anomalous (CTRL – NOBC) BC concentration ($\mu\text{g}/\text{kg}$), cloud fraction (%), and SW heating rates (K/day), respectively, for the pre-monsoon season. Sub-figures (b), (e), and (h) show similar plots for

the monsoon season. Mean vertical profiles of these three anomalies are shown in sub figures (c), (f), and (i), respectively

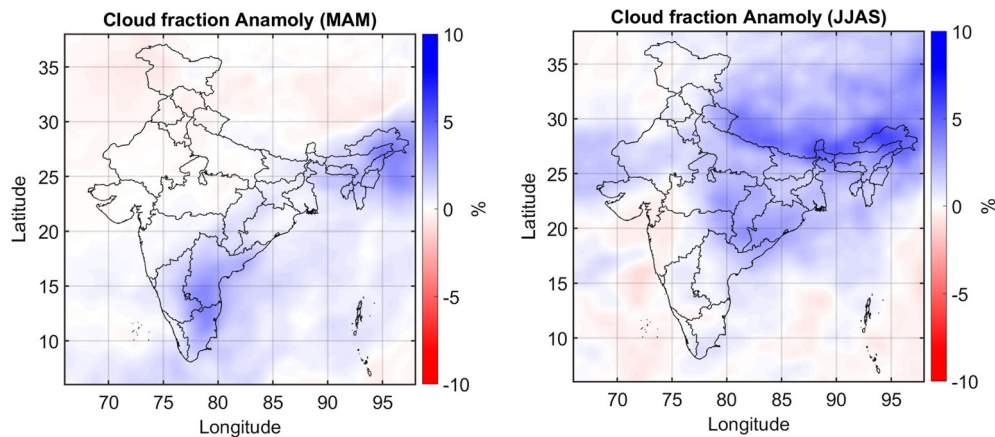


Fig. 9 Spatial plot of cloud fraction (%) anomaly (CTRL – NOBC) during pre-monsoon and monsoon seasons

can be seen during the pre-monsoon season, which is also transported to higher latitudes during the monsoon season.

Spatial plot of mean cloud fraction anomaly is shown in Fig. 9. During pre-monsoon season, over the northeast and southern parts of India, increased cloud fraction is simulated mostly below 30°N due to increased SW heating there. During the monsoon season, positive anomaly is simulated mostly above 15°N and covers most of central and northeast parts of India including IGP.

4.2 Effects on radiation

BC causes strong negative SW radiative forcing at the surface by absorbing incoming SW radiation in the lower troposphere as shown in the previous section. Tables 2, 3, and 4 contain anomalies for LW, SW and Total (sum of both) radiation, respectively. Surface, TOA, and Atmosphere represent anomalies at the surface, top of the atmosphere, and within the atmosphere, respectively. The model estimates all sky radiation by considering all aerosols and clouds in the atmosphere, whereas clear sky is computed by ignoring clouds in the atmosphere.

LW forcing at the surface during the pre-monsoon season is always higher than monsoon season, over both land and oceans. This is due to the fact that SW heating stays near the surface during pre-monsoon but lifts to higher altitudes in monsoon (see Fig. 8). Due to positive cloud fraction anomaly, LW forcing at the TOA during all sky days is higher compared to clear sky days. Difference of TOA and surface anomaly is represented by atmospheric anomaly, which is higher during monsoon season, due to smaller surface anomaly in monsoon.

Since SW anomalies are higher in magnitude compared to LW, total radiation anomalies show similarity with the SW anomalies. Over the land regions, total surface anomalies are about -10 W/m^2 and anomalies in the atmosphere are about 18 W/m^2 . Similar anomalies, with lower magnitude, can be seen over the oceans as well.

SW radiation anomaly at surface is always negative, with the highest reaching -16.2 W/m^2 during the pre-monsoon season over the land regions. Similar to LW anomalies, negative SW anomalies at the surface are higher during pre-monsoon season compared to monsoon season. Positive clear sky TOA anomalies are higher than all sky anomalies.

Table 2 Longwave radiation anomaly in W/m^2 (CTRL – NOBC)

	Pre-monsoon		Monsoon	
	Land			
	All sky	Clear sky	All sky	Clear sky
Surface	5.78 ± 0.47	5.29 ± 0.11	2.45 ± 0.17	2.52 ± 0.81
TOA	3.94 ± 0.39	1.03 ± 0.03	2.82 ± 0.20	0.72 ± 0.07
Atmosphere	-1.84 ± 0.61	-4.26 ± 0.12	0.36 ± 0.26	-1.80 ± 0.19
	Ocean			
	All sky	Clear sky	All sky	Clear sky
Surface	2.47 ± 0.39	2.21 ± 0.01	0.19 ± 0.04	0.34 ± 0.80
TOA	2.50 ± 0.28	0.89 ± 0.05	1.50 ± 0.16	-0.01 ± 0.10
Atmosphere	0.03 ± 0.48	-1.31 ± 0.05	1.31 ± 0.16	-0.35 ± 0.81

Ensemble standard deviation is shown along with ensemble mean anomaly

Table 3 Shortwave radiation anomaly in W/m^2 (CTRL – NOBC)

	Pre-monsoon		Monsoon	
	Land			
	All sky	Clear sky	All sky	Clear sky
Surface	-16.20 ± 0.06	-14.86 ± 0.46	-13.25 ± 0.10	-12.74 ± 0.37
TOA	4.00 ± 0.21	6.14 ± 0.04	3.80 ± 0.13	6.34 ± 0.08
Atmosphere	20.20 ± 0.22	21.00 ± 0.46	17.06 ± 0.16	19.07 ± 0.13
	Ocean			
	All sky	Clear sky	All sky	Clear sky
Surface	-10.95 ± 0.27	-9.84 ± 0.35	-7.10 ± 0.24	-7.27 ± 0.17
TOA	0.53 ± 0.12	2.12 ± 0.08	0.78 ± 0.25	1.71 ± 0.06
Atmosphere	11.48 ± 0.30	11.97 ± 0.36	7.88 ± 0.35	8.98 ± 0.18

Ensemble standard deviation is shown along with ensemble mean anomaly

Due to strong SW heating in the atmosphere, a large positive SW anomaly in the atmosphere is simulated, which stays between 17 to 21 W/m^2 over the land regions and 8 to 12 W/m^2 over the oceans.

Net reduction of radiation at the surface is higher than previous modeling studies conducted with BC aerosols. Meehl et al. (2008) found a net decrease of -6.5 W/m^2 over land regions, whereas a larger decrease of -12.6 W/m^2 ($-12.3 \text{ SW} + 8.7 \text{ LW}$) was found by Lau et al. (2006), which could be due to inclusion of dust aerosols.

Vertical profiles of all sky radiation, averaged over land and ocean regions during the pre-monsoon and monsoon season are shown in Fig. 10. Filled and empty markers represent downward and upward radiation anomalies respectively. LW and SW anomalies are shown in red and blue, respectively. The shading along with anomalies represents ensemble standard deviation.

Higher SW heating near the surface during the pre-monsoon season results in higher downward LW radiation

at the surface compared to the monsoon season (see Fig. 8e and f.). This can also be seen in the vertical profiles of downward LW radiation, which shows about 4 W/m^2 downward LW radiation anomaly during the pre-monsoon season which is absent during the monsoon season. However, due to northward migration of ITCZ, heating exists at a height of 8–10 km during monsoon season.

SW anomalies are always negative (both upward and downward) and asymptotically approach 0 at the TOA from -20 W/m^2 at the surface. Upward SW anomalies are also negative to balance the downward anomalies.

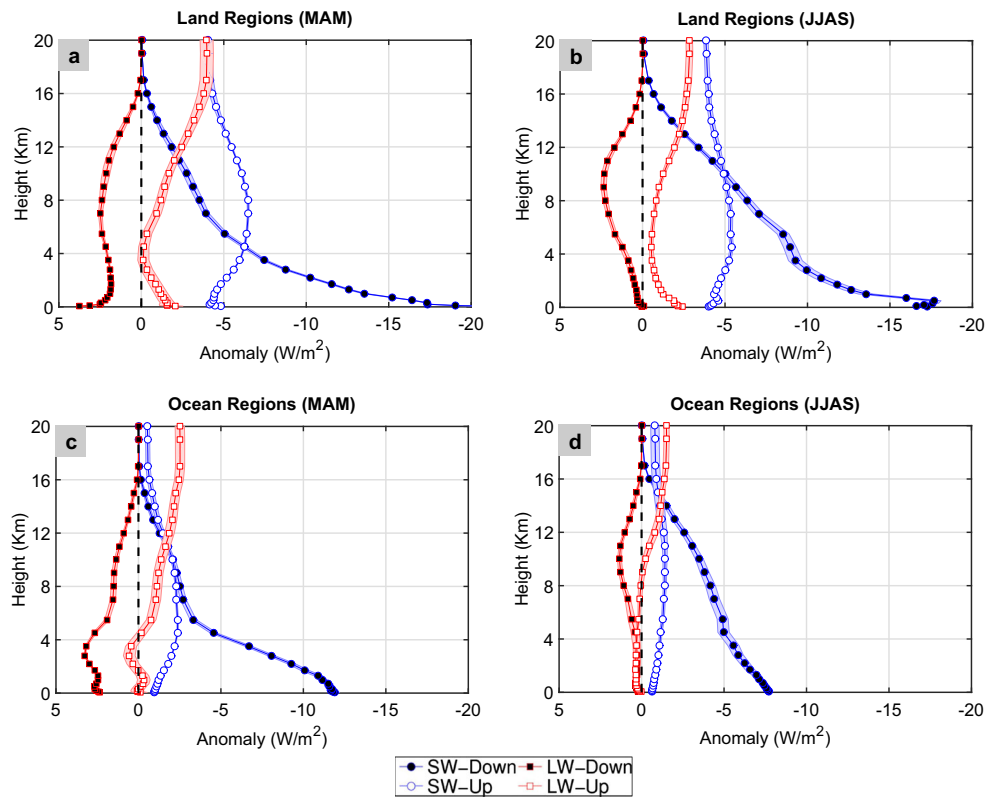
Figure 11 shows the vertical profiles of net (downward-upward) radiation anomalies for LW, SW, and total anomalies. During the pre-monsoon season, net cooling persists up to height of 4 km, over both ocean and land regions. However, during the monsoon season, it reaches up to height of 6 and 12 km over land and oceans, respectively. Due to larger SW anomalies compared to LW, Total anomalies resemble the SW anomalies.

Table 4 Total radiation anomaly in W/m^2 (CTRL – NOBC)

	Pre-monsoon		Monsoon	
	Land			
	All sky	Clear sky	All sky	Clear sky
Surface	-10.42 ± 0.47	-9.57 ± 0.48	-10.80 ± 0.20	-10.21 ± 0.89
TOA	7.94 ± 0.44	7.17 ± 0.05	6.62 ± 0.24	7.06 ± 0.11
Atmosphere	18.36 ± 0.65	16.74 ± 0.48	17.42 ± 0.31	17.28 ± 0.23
	Ocean			
	All sky	Clear sky	All sky	Clear sky
Surface	-8.48 ± 0.48	-7.64 ± 0.36	-6.90 ± 0.24	-6.93 ± 0.82
TOA	3.03 ± 0.31	3.02 ± 0.10	2.29 ± 0.30	1.70 ± 0.12
Atmosphere	11.51 ± 0.57	10.66 ± 0.37	9.19 ± 0.38	8.64 ± 0.83

Ensemble standard deviation is shown along with ensemble mean anomaly

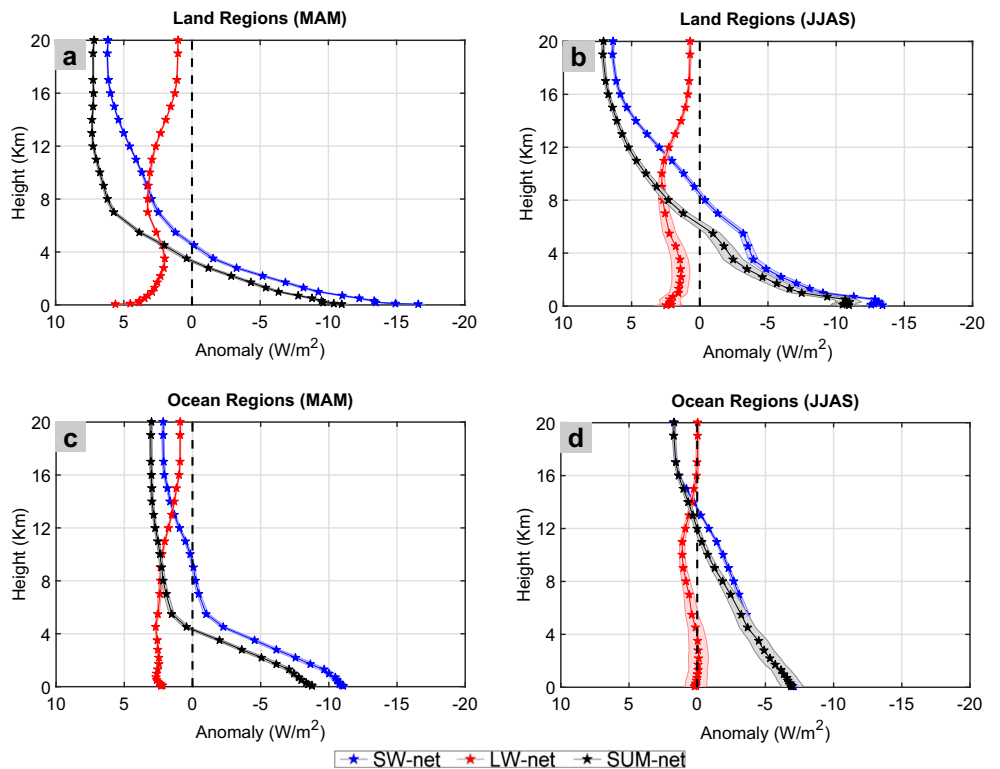
Fig. 10 Vertical profiles of all sky Shortwave and Longwave radiation anomaly (a, b) land regions for pre-monsoon season; (c, d) same for ocean regions. Shading along the curve represents ensemble standard deviation



Spatial plots of net surface radiation anomalies are shown in Fig. 12. Negative SW and positive LW anomalies can be seen all over the domain with higher magnitude

concentrated over IGP during monsoon season, due to presence of higher aerosols and cloud amounts there (see Fig. 11e, f).

Fig. 11 Similar to Fig. 10 but showing net SW, LW and total radiation anomaly



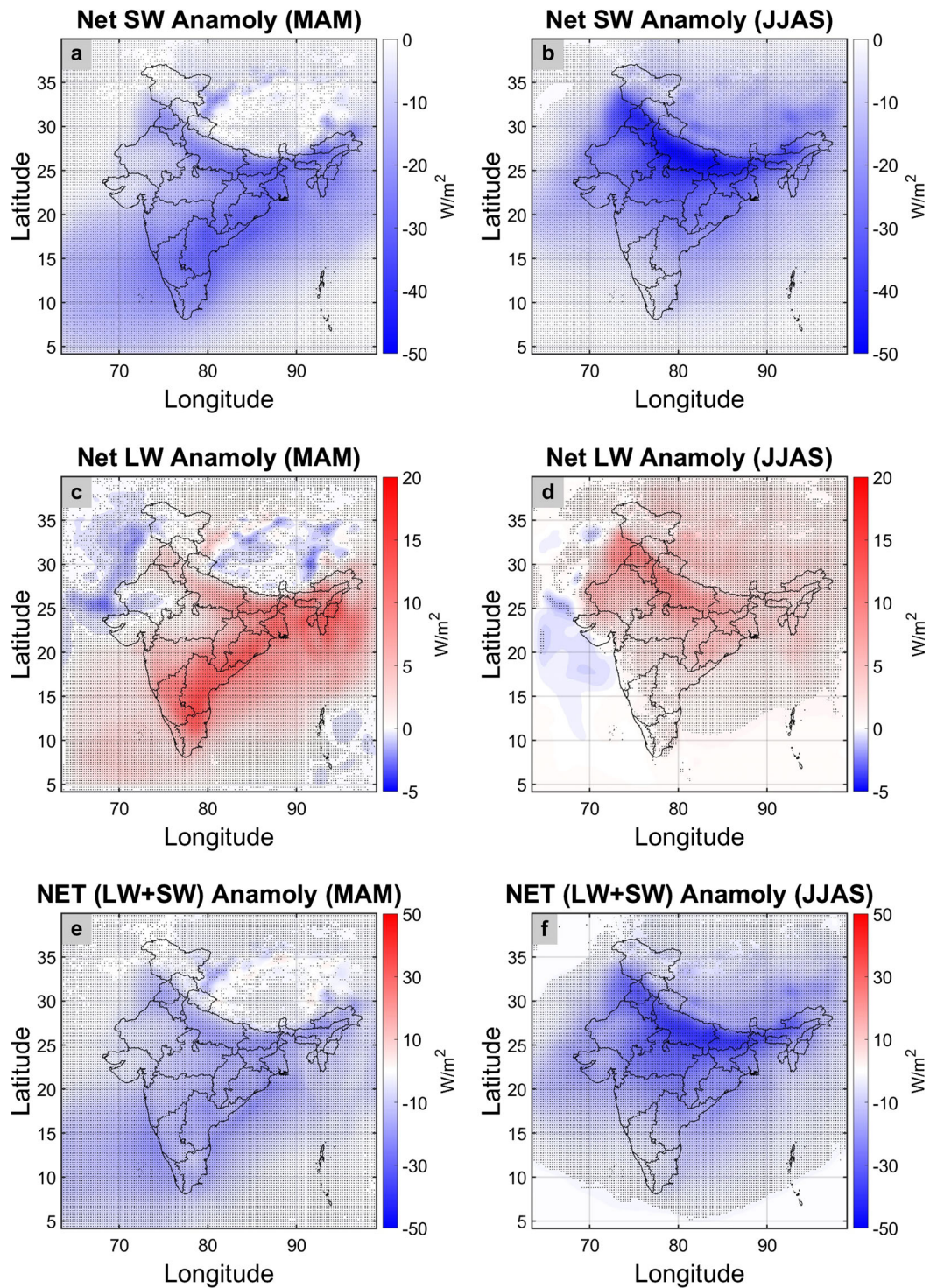


Fig. 12 Spatial plots of radiation anomaly at the surface. **a, b** Shortwave for pre-monsoon and monsoon season. **c, d** Similar plots for LW. **f, e** Sum of SW and LW. Stippling indicates areas where ensemble mean divided by ensemble standard deviation exceeds 1

4.3 Effects on temperature

Temperature is directly affected by the radiation anomalies. Figure 13a, b show the surface temperature anomaly for the pre-monsoon and monsoon seasons, respectively. During

the pre-monsoon season, most parts of Indian land surface are cooling, except Himalayas and some desert regions in Rajasthan. However, during the monsoon season, surface cooling is present over entire land region. Warming over Bay of Bengal can be noticed in both seasons.

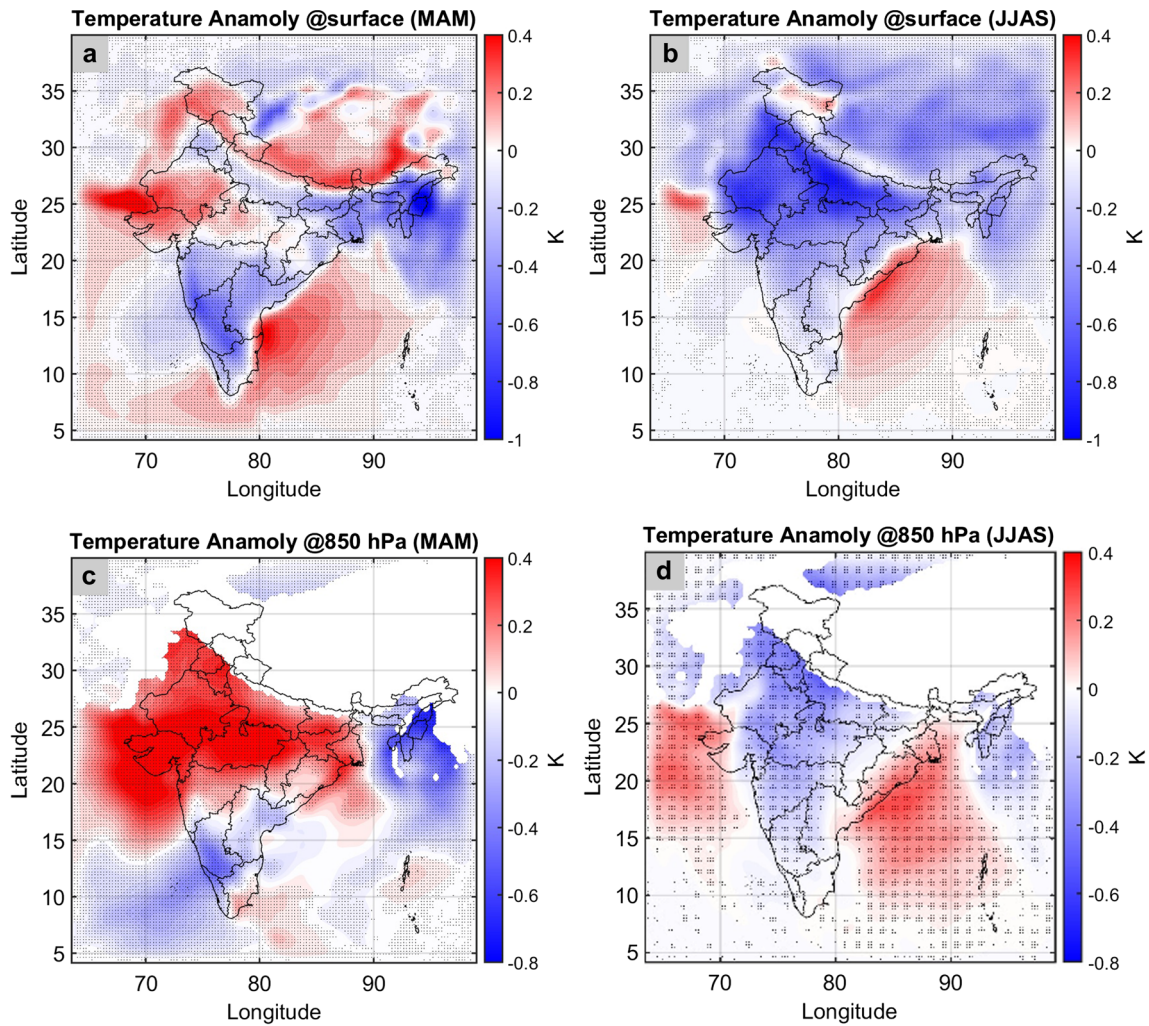


Fig. 13 a, b Spatial plots of temperature anomaly at surface during pre-monsoon and monsoon season. c, d Same as (a, b) but at 850 hPa. Stippling indicates areas where ensemble mean divided by ensemble standard deviation exceeds 1

Figure 13c, d show temperature anomalies plots at 850 hPa pressure level. A consistent warming over most parts of India can be seen during the pre-monsoon season, whereas,

during the monsoon season, warming can be noticed only over the Bay of Bengal, while other land regions are still cooling.

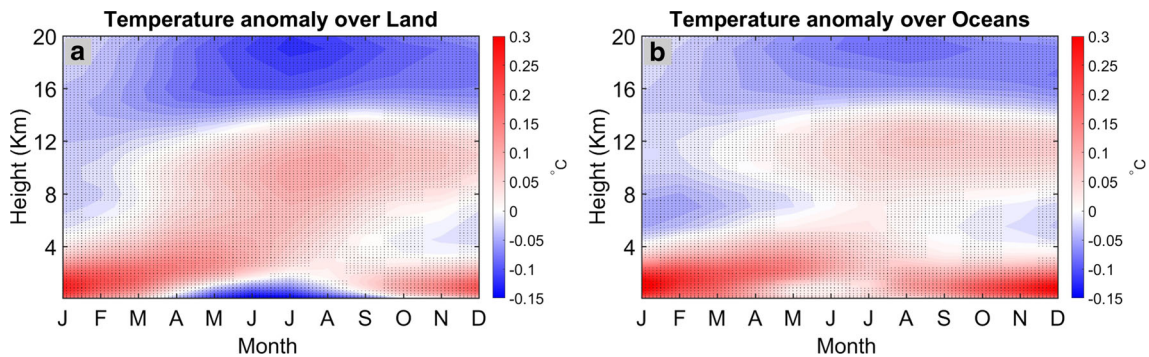


Fig. 14 Mean timeseries of temperature anomaly with height (a) land and (b) ocean. Stippling indicates areas where ensemble mean divided by ensemble standard deviation exceeds 1

Figure 14a, b show monthly time series of temperature anomalies with altitude, averaged over land and oceans, respectively. From January to March, a positive surface temperature anomaly is simulated over both land and oceans. However, with the northward advancement of the ITCZ across India, and the associated increase in convective

activity, aerosols and thus heating, rise above the ground level and a surface cooling can be seen from April to September over land regions. Due to less convection over oceans, this phenomenon is absent there and warming persists. With ITCZ shifting back to Indian Ocean in October, cooling phenomenon disappears over land regions.

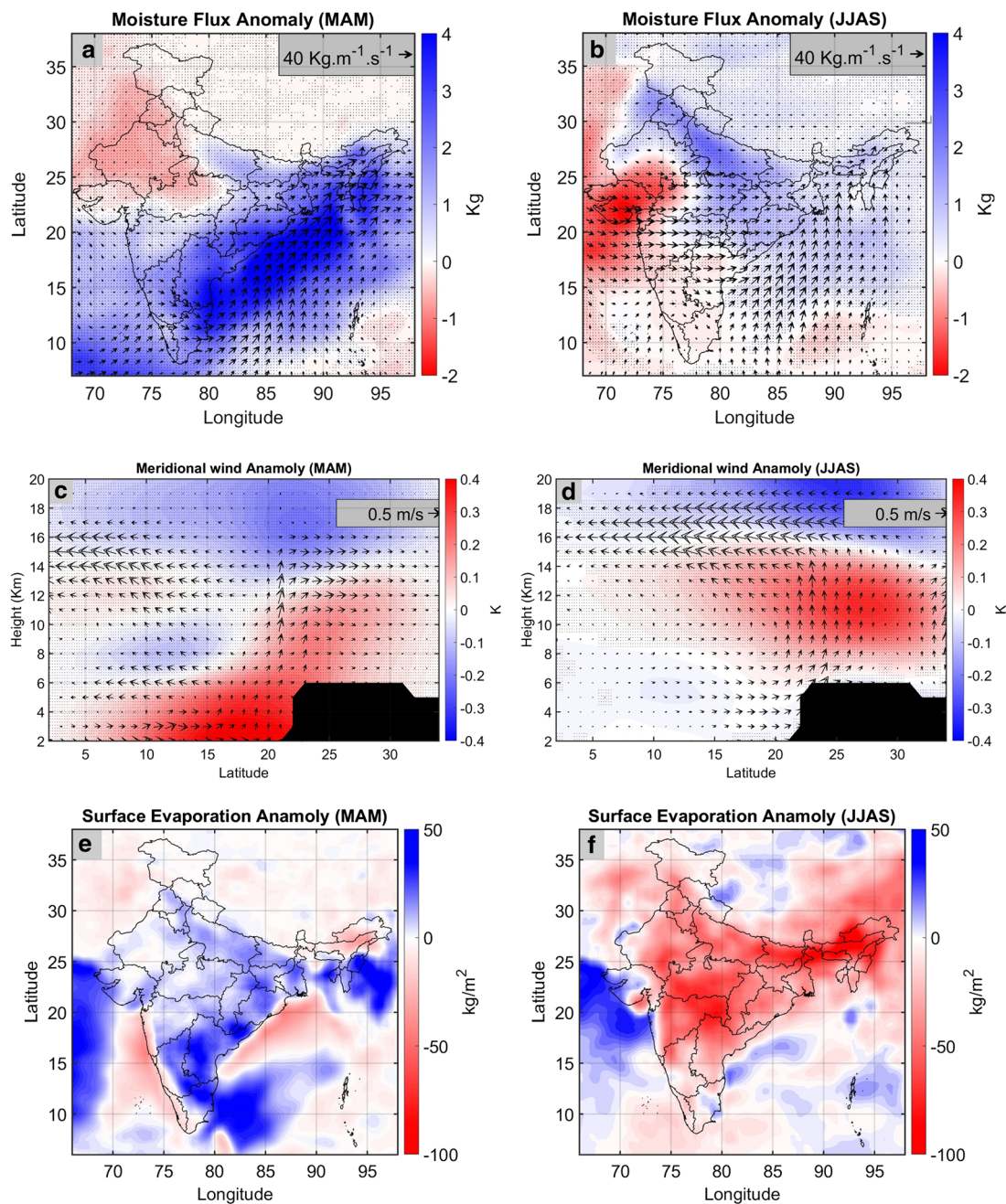


Fig. 15 Effect of BC on moisture transport and wind circulation (a) and (b) vertically integrated moisture flux anomaly for MAM and JJAS (c) and (d) Meridional circulation and temperature anomaly averaged between 65-99E for MAM and JJAS (units of meridional velocity

and omega are 1 m/s and 10^{-2} m/s respectively). Stippling indicates areas where ensemble mean divided by ensemble standard deviation exceeds 1. e, f Total surface evaporation anomaly for pre-monsoon and monsoon season, respectively

4.4 Effects on winds and moisture transport

Winds and moisture anomalies are affected by the temperature anomalies. Figure 15a, b shows the vertically integrated moisture flux (Q) anomalies along with water vapor (q) anomalies during the pre-monsoon and monsoon seasons, respectively. Flux is calculated by,

$$Q = -\frac{1}{g} \int_{p_{surf}}^{p_{top}} qV dp \quad (1)$$

where p is the air pressure, p_{surf} is the surface pressure, p_{top} is pressure at the top of the atmosphere, taken to be at 50 hPa where q becomes negligible, g is the acceleration due to gravity, 9.8 m/s^2 , and V is the horizontal wind vector defined as

$$V = ui + vj \quad (2)$$

with u and v being the eastward and northward wind components, respectively. Because of the heating over most parts of India, an increased transport of moisture from Bay of Bengal and Indian Ocean to northeast India is simulated during the pre-monsoon season. Moreover, during the monsoon season, an increased westerly moisture flux anomaly over India is simulated, which occurs due to the dipole heating between Bay of Bengal (heating) and entire India (cooling) at 850 hPa level (see Fig. 13).

Figure 15c, d shows meridional wind anomaly (zonal average between 75E-95E) along with temperature contours during pre-monsoon and monsoon seasons, respectively.

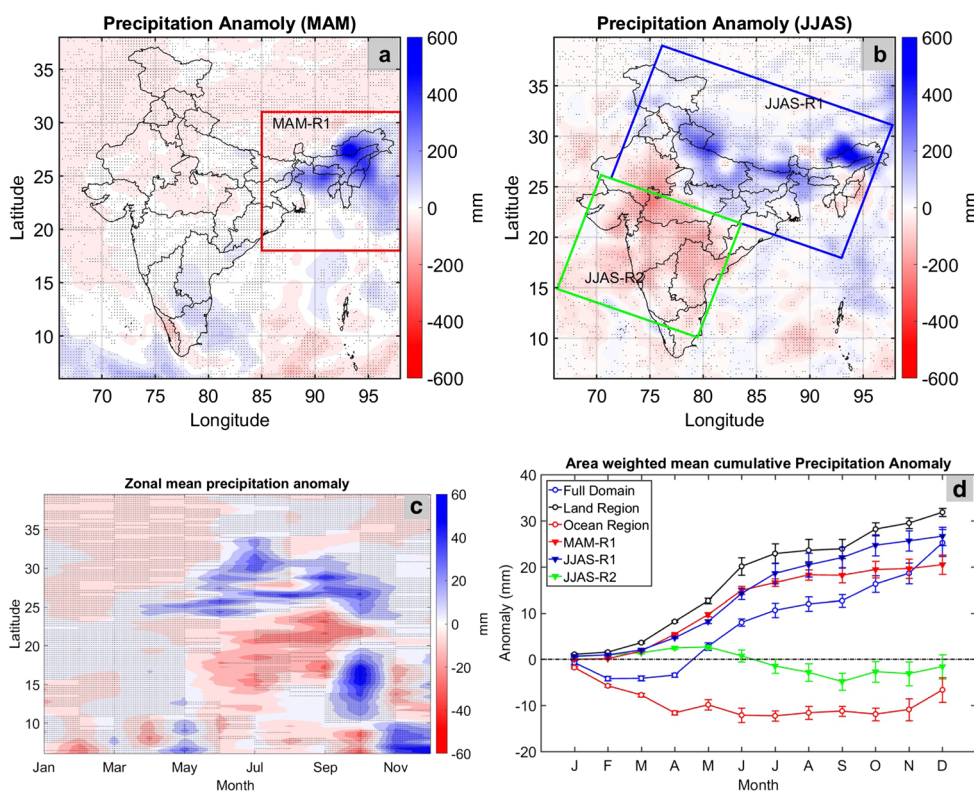
During the pre-monsoon season, SW heating in the lower troposphere, between 10 to 20 N latitude, causes a southerly meridional wind anomaly near surface. Lifting of the wind takes place near 15 N and then it divides into two branches at higher altitudes, toward north and south, respectively. However, during the monsoon season, since the heating is concentrated at higher altitudes and latitudes (20–30 N), the convection takes place further to the north (25 N).

Surface evaporation anomalies are shown in Fig. 15e, f during the pre-monsoon and monsoon seasons, respectively. Due to consistent heating over the Bay of Bengal (see Fig. 14a, b), an increased evaporation anomaly can be seen in both the seasons. This positive evaporation anomaly enhances the moisture transport over India. Also, due to land surface cooling over India, a decreased evaporation is simulated there during the monsoon season.

4.5 Effects on precipitation

Spatial plots of precipitation anomalies are shown in Fig. 16a, b during the pre-monsoon and monsoon seasons, respectively. Few regions of interest are marked in the sub-figures, which are MAM-R1 (red rectangle in Fig. 16a), JJAS-R1 (Blue parallelogram in Fig. 16b) and JJAS-R2 (Green parallelogram in Fig. 16b).

Fig. 16 Effect of BC on Precipitation. **a, b** Spatial plot of precipitation anomaly for pre-monsoon and monsoon season. Three regions are marked in these figures, namely MAM-R1, JJAS-R1, and JJAS-R2. **c** Zonal mean precipitation anomaly over different regions (full domain, oceans, land, and three regions marked in (a) and (b)). Stippling in the figures indicate areas where ensemble mean divided by ensemble standard deviation exceeds 1



Because of the moisture flux anomaly from Bay of Bengal and Indian Ocean along with increased evaporation over the Bay of Bengal (see Fig. 15), an increased precipitation anomaly over the region MAM-R1 can be seen during the pre-monsoon season which resembles the increased cloud fraction there (Fig. 9). The decreased precipitation anomaly over JJAS-R2 during the monsoon season can be attributed to increased westerly moisture flux anomaly over central India which transports moisture from JJAS-R2 to JJAS-R1 (see Fig. 15b). This reduction is further substantiated by the reduced evaporation over JJAS-R2 (Fig. 15f).

Figure 16c shows the zonal average monthly time series of precipitation anomaly. Consistent with the spatial plots, an increased precipitation anomaly between 25°N to 35°N is simulated during March to October, which is due to moisture transport from southern regions (15°N to 25°N).

Time series of area-weighted mean cumulative precipitation anomalies are plotted in Fig. 16d for different regions. Ensemble standard deviation is represented by error-bars in the figure. Rainfall over land regions, JJAS-R1 and MAM-R1 increases consistently. However, over the region JJAS-R2, a small increasing trend until May can be seen, which starts to decrease till September, and then increases again. Over the oceans, a consistent decreasing trend until monsoon can be seen, which stays constant and increases as winter approaches. Over the full domain, a consistent increase throughout the year can be seen, with the highest increase during pre-monsoon and winter.

Table 5 shows percentage of rainfall anomalies over different regions. Even though magnitude of anomalies during the pre-monsoon and monsoon seasons are similar (see Fig. 16d), percentage change during the pre-monsoon season is larger. Increase of rainfall can be as much as 42% over

MAM-R1 (during March) and a decrease of about 5–8% can be seen over JJAS-R2, during the monsoon season.

5 Summary and conclusion

The present study is probably the first attempt to assess the radiative effects of ‘black carbon’ aerosols using a high-resolution regional climate model ‘WRF-Chem’ with aerosol and chemistry feedbacks coupled to meteorology. Previous studies conducted with other regional climate models have focused on ‘all anthropogenic’ forcing, instead of solely BC. We have also included the wet scavenging process of aerosols (aerosol washout effect by rainfall), in the absence of which, aerosols reach much higher altitudes during the monsoon season, which may not be realistic. Our main objective was to incorporate only the radiative effects of BC aerosols (by excluding the indirect effects), while keeping wet-scavenging option ‘on,’ which required few modifications in the model code. The ‘mixactivate’ routine of the model, which is responsible for the aerosol CCN activities, was turned ‘off’.

Simulations were conducted with WRF-Chem version 3.4.1 for the year 2010. Simulated climatic variables (AOD, BC concentration, winds, precipitation, and temperature) were compared to satellite and in situ observations and it was found that the model performs adequately well, when compared to previous studies on evaluation of WRF-Chem model (Govardhan et al. 2016; Kumar et al. 2012; Michael et al. 2014; Seethala et al. 2011).

After thorough evaluation of the model with different configurations, two sets of experiments were performed. One control experiment (CTRL) in which all aerosol emissions were included and in another experiment, BC

Table 5 Precipitation anomaly over different regions

% Anomaly	All domain	Land	Ocean	MAM-R1	JJAS-R1	JJAS-R2
Jan	-1.29 ± 0.75	3.26 ± 1.73	-3.98 ± 0.65	-0.42 ± 6.12	21.08 ± 4.08	16.34 ± 4.64
Feb	-7.46 ± 0.33	-2.27 ± 0.60	-12.68 ± 0.49	16.02 ± 2.25	4.89 ± 0.53	29.48 ± 2.78
Mar	0.13 ± 0.23	9.86 ± 0.47	-6.60 ± 0.40	42.02 ± 0.67	19.00 ± 0.55	45.67 ± 1.77
Apr	0.74 ± 0.43	7.69 ± 0.38	-5.73 ± 0.66	36.78 ± 0.21	23.08 ± 0.39	42.64 ± 0.95
May	3.85 ± 0.53	4.49 ± 1.01	2.21 ± 1.06	18.82 ± 1.74	14.18 ± 4.33	11.25 ± 5.48
Jun	2.15 ± 0.27	4.02 ± 1.76	-2.04 ± 1.38	12.28 ± 2.36	11.62 ± 1.62	-7.65 ± 4.78
Jul	0.89 ± 0.42	0.19 ± 0.59	-0.44 ± 0.53	3.60 ± 1.18	6.64 ± 1.65	-5.07 ± 1.64
Aug	0.61 ± 0.09	-0.27 ± 0.32	0.90 ± 0.61	4.12 ± 1.41	3.66 ± 1.37	-4.48 ± 3.07
Sep	0.38 ± 0.47	-1.01 ± 0.41	0.85 ± 1.12	-0.21 ± 2.20	2.77 ± 0.86	-7.20 ± 1.67
Oct	3.04 ± 1.28	5.03 ± 3.11	0.82 ± 1.46	4.40 ± 6.71	-0.71 ± 3.66	23.67 ± 12.35
Nov	1.93 ± 1.11	2.49 ± 0.89	-0.01 ± 1.02	4.59 ± 21.84	18.09 ± 9.81	-1.34 ± 2.99
Dec	5.88 ± 0.96	7.99 ± 0.72	4.62 ± 1.45	12.76 ± 1.76	18.96 ± 3.45	11.40 ± 2.11

Ensemble standard deviation is shown along with ensemble mean anomaly

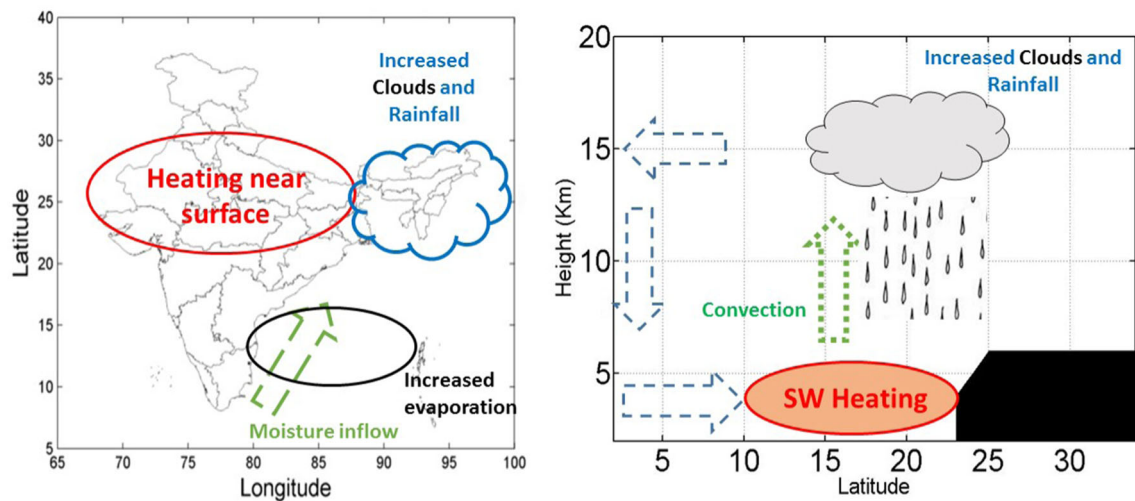
emissions were set to zero (NOBC). Each experiment was conducted with five ensemble simulations (with different initial conditions) to quantify model uncertainties.

It was found that before the onset of monsoon season, most of the BC concentration remains near the surface and strong absorption of incoming SW radiation takes place, which induces a net negative surface forcing (-10 W/m^2) and positive atmospheric forcing (18 W/m^2) over land regions, which in turn heats the lower troposphere (Fig. 8d). Lower tropospheric heating during pre-monsoon season causes convection below 30°N and increases cloud fraction there (see Fig. 8g), thus enhancing meridional circulation (see Fig. 15c), leading to increased precipitation over northeast regions (MAM-R1) of India during this season. This increase can be as much as 42% in the month of March

(Table 5). Along with this, we also noted an increased evaporation over oceans, which substantiates the enhancement of pre-monsoon rainfall.

During the monsoon season, with the advancement of ITCZ over India in the month of June, BC aerosols, and thus SW heating, rise to higher levels and further to north, over the land regions (see Fig. 8), which results in near surface cooling instead of heating (Fig. 14a). In contrast to this cooling, warming persists over Bay of Bengal (due to less convection, Fig. 14b) creating a land-sea thermal gradient between India and Bay of Bengal (a dipole heating phenomenon). Thus, in addition to increased southerly moisture anomaly from Bay of Bengal, dipole heating results in an increased westerly moisture flux anomaly over India. Along with this, an increased cloud fraction can be seen

BC-Rainfall Interaction during pre-monsoon season



BC-Rainfall Interaction during monsoon season

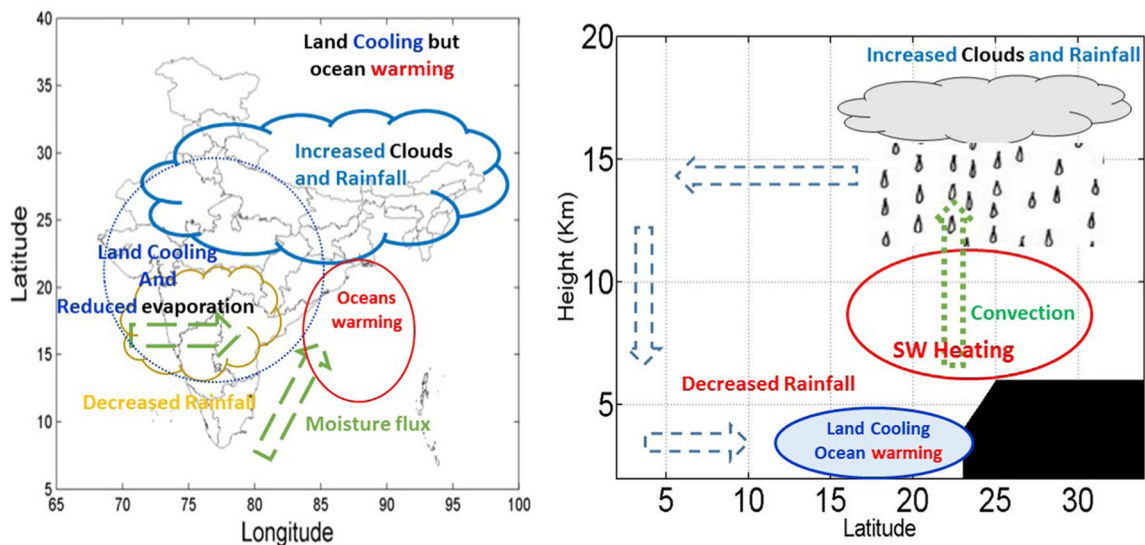


Fig. 17 Cartoon illustration of BC-Rainfall interactions during pre-monsoon and monsoon season

over higher latitudes (Figs. 8h and 9). Overall, we found an increased precipitation anomaly over north and northeast regions of India (JJAS-R1), and a decrease over southern parts of India (JJAS-R2) as shown in Fig. 16. The decreased rainfall over this region can be explained by two factors, one is the reduced evaporation due to cooling of land regions (see Fig. 15f) and the other, increased westerly moisture flux anomaly (see Fig. 15a).

The overall process by which BC aerosols affect precipitation during pre-monsoon season can be summarized in a cartoon schematic as shown in Fig. 17. BC absorption over IGP creates lower tropospheric heating which results into increased convection near 15–20°N causing increased cloud fraction and meridional circulation. Circulation anomaly along with increased evaporation over oceans results into moisture inflow from southern regions to create a positive rainfall anomaly over northeast India. Due to northward migration of ITCZ during the monsoon season, SW heating at higher altitudes occurs over the land regions (cooling there with reduced evaporation) but oceans still show warming. This dipole heating leads to increased moisture flux anomaly which decreases precipitation over south India and increases over north and northeast India.

In this study, we propose a new mechanism through which BC aerosols affect Indian summer monsoon. Increased precipitation anomaly over north-east regions of India due to southerly moisture flux anomaly is similar to EHP mechanism (Lau et al. 2006; Meehl et al. 2008). However, decreased precipitation over southern part of India (JJAS-R2) and increase over northern part (JJAS-R1), due to dipole heating phenomenon and westerly moisture flux anomaly along with evaporation changes, has not been reported in previous studies. This is probably due to the fact that with high resolution models, regional features and processes are simulated more accurately than by coarse resolution GCM models.

With growing industrialization and population over IGP, effect of increasing BC aerosols will be opposite to that of other scattering type of aerosols which causes a weakening of Indian summer monsoon as shown in previous studies by Bollasina et al. (2011), Das et al. (2016), and Randles and Ramaswamy (2008).

Aerosol-rainfall interactions are complex phenomena, which can get even more complicated with inclusion of indirect effects. Therefore, to understand the overall process of these interactions, further experiments with inclusion of all aerosol effects should be conducted. More sensitivity studies, with different emission inventories, aerosol microphysical parameterizations, or emission scaling experiments, are required to test whether the model responses found here scale linearly.

Acknowledgments The MODIS and TRMM data used in this study were produced with the Giovanni online data system, developed and maintained by the National Aeronautics and Space Administration (NASA) GES DISC. We acknowledge the MODIS and TRMM teams for the data used. We thank the PIs for their efforts in establishing and maintaining the AERONET sites at Kanpur, Jaipur, Nainital, and Gandhi College. The NCEP FNL reanalysis data were downloaded from <http://rda.ucar.edu/datasets/ds083.2/> and the ERA-Interim data were downloaded from the UCAR website <http://rda.ucar.edu/datasets/ds627.0>. We also acknowledge Mr. Shamjad, PhD student at IIT Kanpur for providing useful BC concentration data. We thank the anonymous reviewer for critically reading the manuscript and suggesting substantial improvements. We gratefully acknowledge the financial support for HPC server by the Earth System Science Organization, Ministry of Earth Sciences, Government of India (MOES/16/05/11-RDEAS) and funding support by Indo-UK Monsoon project, Ministry of Earth Sciences, Government of India (MoES/NERC/16/02110 PC-) and Climate Change Program, Department of Science and Technology to conduct this research work.

References

- Ackerman A, Toon O, Stevens D, Heymsfield A, Ramanathan V, Welton E (2000) Reduction of tropical cloudiness by soot. *Science* 288(5468):1042–1047
- Ackermann I, Hass H, Memmesheimer M, Ebel A, Binkowski F, Shankar U (1998) Modal aerosol dynamics model for Europe: development and first applications. *Atmos Environ* 32(17):2981–2999. doi:10.1016/S1352-2310(98)00006-5, <http://www.sciencedirect.com/science/article/pii/S1352231098000065>
- Babu S, Manoj M, Moorthy K, Gogoi M, Nair V, Kompalli S, Satheesh S, Niranjana K, Ramagopal K, Bhuyan P, et al. (2013) Trends in aerosol optical depth over Indian region: Potential causes and impact indicators. *Journal of Geophysical Research: Atmospheres* 118(20)
- Bollasina M, Nigam S, Lau K (2008) Absorbing aerosols and summer monsoon evolution over south Asia: an observational portrayal. *J Clim* 21(13):3221–3239
- Bollasina M, Ming Y, Ramaswamy V (2011) Anthropogenic aerosols and the weakening of the South Asian summer monsoon. *Science* 334(6055):502–505. doi:10.1126/science.1204994
- Chung C, Ramanathan V (2006) Weakening of north Indian SST gradients and the monsoon rainfall in India and the Sahel. *J Clim* 19(10):2036–2045
- Chung C, Ramanathan V, Kiehl J (2002) Effects of the South Asian absorbing haze on the northeast monsoon and surface–air heat exchange. *J Climate* 15(17):2462–2476. doi:10.1175/1520-0442(2002)015<2462:EOTSAA>2.0.CO;2
- Collins W, Rasch P, Eaton B, Fillmore D, Kiehl J, Beck C, Zender C (2002) Simulation of aerosol distributions and radiative forcing for IndoEX: Regional climate impacts. *Journal of Geophysical Research: Atmospheres* 107(D19):INX2 27–1–INX2 27–20. doi:10.1029/2000JD000032
- Das S, Dey S, Dash S (2015a) Impacts of aerosols on dynamics of Indian summer monsoon using a regional climate model. *Clim Dyn* 44(5–6):1685–1697
- Das S, Dey S, Dash S, Giuliani G, Solmon F (2015b) Dust aerosol feedback on the Indian summer monsoon: Sensitivity to absorption property. *J Geophys Res Atmos* 120(18):9642–9652
- Das S, Dey S, Dash S (2016) Direct radiative effects of anthropogenic aerosols on Indian summer monsoon circulation. *Theor Appl Climatol* 124(3–4):629–639

- Dee D, Uppala S, Simmons A (2011) The era-interim reanalysis: Configuration and performance of the data assimilation system. *Quarterly Journal of the Royal Meteorological Society*. doi:[10.1002/qj.828](https://doi.org/10.1002/qj.828)
- Flato G, Marotzke J, Abiodun B, Braconnot P, Chou S, Collins W, Cox P, Driouech F, Emori S, Eyring V, et al. (2013) Evaluation of climate models. In: *Climate change 2013: The physical science basis. contribution of working group I to the fifth assessment report of the intergovernmental panel on climate change*. *Climate change 2013 5*, pp 741–866
- Ganguly D, Jayaraman A, Rajesh T, Gadhavi H (2006) Wintertime aerosol properties during foggy and nonfoggy days over urban center delhi and their implications for shortwave radiative forcing. *Journal of Geophysical Research: Atmospheres* 111(D15)
- Ganguly D, Rasch P, Wang H, Yoon J (2012a) Climate response of the south asian monsoon system to anthropogenic aerosols. *Journal of Geophysical Research: Atmospheres* 117(D13)
- Ganguly D, Rasch P, Wang H, Yoon J (2012b) Fast and slow responses of the south asian monsoon system to anthropogenic aerosols. *Geophys Res Lett* 39(18):118804. doi:[10.1029/2012GL053043](https://doi.org/10.1029/2012GL053043)
- Gautam R, Hsu N, Tsay S, Lau K, Holben B, Bell S, Smirnov A, Li C, Hansell R, Ji Q, et al. (2011) Accumulation of aerosols over the indo-gangetic plains and southern slopes of the himalayas: distribution, properties and radiative effects during the 2009 pre-monsoon season. *Atmos. Chem. Phys.* 11(24):12,841–12,863
- Giles D, Holben B, Tripathi S, Eck T, Newcomb W, Slutsker I, Dickerson R, Thompson A, Mattoo S, Wang S, et al. (2011) Aerosol properties over the indo-gangetic plain: a mesoscale perspective from the tigerz experiment. *Journal of Geophysical Research: Atmospheres* 116(D18)
- Govardhan G, Nanjundiah R, Sathesh S, Moorthy K, Takemura T (2016) Inter-comparison and performance evaluation of chemistry transport models over Indian region. *Atmos Environ* 125:486–504
- Grell G, Peckham S, Schmitz R, McKeen S (2005) Fully coupled "online" chemistry within the wrf model. *Atmospheric Environment*. <http://www.sciencedirect.com/science/article/pii/S1352231005003560>
- Han J, Pan H (2011) Revision of convection and vertical diffusion schemes in the ncep global forecast system. *Weather Forecast* 26(4):520–533. doi:[10.1175/WAF-D-10-05038.1](https://doi.org/10.1175/WAF-D-10-05038.1)
- Hansen J, Sato M, Ruedy R (1997) Radiative forcing and climate response. *J Geophys Res* 102(D6):6831. doi:[10.1029/96JD03436](https://doi.org/10.1029/96JD03436)
- Harris I, Jones P, Osborn T, Lister D (2014) Updated high-resolution grids of monthly climatic observations – the cru ts3.10 dataset. *Int J Climatol* 34(3):623–642. doi:[10.1002/joc.3711](https://doi.org/10.1002/joc.3711)
- Henriksson S, Laaksonen A, Kerminen V, Räisänen P, Järvinen H, Sundström AM, Gd L (2011) Spatial distributions and seasonal cycles of aerosols in India and China seen in global climate-aerosol model. *Atmos Chem Phys* 11(15):7975–7990. doi:[10.5194/acp-11-7975-2011](https://doi.org/10.5194/acp-11-7975-2011)
- Holben B, Eck T, Slutsker I, Tanré D, Buis J, Setzer A, Vermote E, Reagan JA, Kaufman YJ, Nakajima T, Lavenu F, Jankowiak I, Smirnov A (1998) Aeronet—a federated instrument network and data archive for aerosol characterization. *Remote Sens Environ* 66(1):1–16. doi:[10.1016/S0034-4257\(98\)00031-5](https://doi.org/10.1016/S0034-4257(98)00031-5)
- Iacono M, Delamere J, Mlawer E, Shephard M, Clough S, Collins WD (2008) Radiative forcing by long-lived greenhouse gases: Calculations with the aer radiative transfer models. *J Geophys Res Atmos* 113(D13):n/a–n/a. doi:[10.1029/2008JD009944](https://doi.org/10.1029/2008JD009944)
- IMD (2010) India meteorological department, annual report 2010. <http://metnet.imd.gov.in/imdnews/ar2010.pdf>
- Jacobson M (2002) Control of fossil fuel particulate black carbon and organic matter, possibly the most effective method of slowing global warming. *J Geophys Res Atmos* (19842012) 107(D19). doi:[10.1029/2001JD001376](https://doi.org/10.1029/2001JD001376)
- Kaufman Y, Koren I (2006) Smoke and pollution aerosol effect on cloud cover. *Science* 313(5787):655–658
- Kumar R, Naja M, Pfister G, Barth M, Wiedinmyer C, Brasseur G (2012) Simulations over south asia using the weather research and forecasting model with chemistry (wrf-chem): chemistry evaluation and initial results. *Geosci Model Dev* 5(3):619–648
- Lau K, Kim M, Kim K (2006) Asian summer monsoon anomalies induced by aerosol direct forcing: the role of the tibetan plateau. *Clim Dyn* 26(7-8):855–864
- Lelieveld J, Crutzen P, Ramanathan V, Andreae M, Brenninkmeijer C, Campos T, Cass G, Dickerson R, Fischer H, De Gouw J, et al. (2001) The Indian ocean experiment: widespread air pollution from south and southeast asia. *Science* 291(5506):1031–1036
- Lu Z, Zhang Q, Streets D (2011) Sulfur dioxide and primary carbonaceous aerosol emissions in China and India, 1996–2010. *Atmos Chem Phys* 11(18):9839–9864
- Manoj M, Devara P, Safai P, Goswami B (2011) Absorbing aerosols facilitate transition of Indian monsoon breaks to active spells. *Clim Dyn* 37(11-12):2181–2198
- Meehl G, Arblaster J, Collins W (2008) Effects of Black Carbon Aerosols on the Indian Monsoon. *Journal of Climate*. doi:[10.1175/2007JCLI1777.1](https://doi.org/10.1175/2007JCLI1777.1)
- Menon S, Hansen J, Nazarenko L, Luo Y (2002) Climate effects of black carbon aerosols in china and india. *Science* 297(5590):2250–2253. doi:[10.1126/science.1075159](https://doi.org/10.1126/science.1075159), <http://science.sciencemag.org/content/297/5590/2250>, <http://science.sciencemag.org/content/297/5590/2250.full.pdf>
- Menon S, Koch D, Beig G, Sahu S, Fasullo J, Orlikowski D (2010) Black carbon aerosols and the third polar ice cap. *Atmos Chem Phys* 10(10):4559–4571. doi:[10.5194/acp-10-4559-2010](https://doi.org/10.5194/acp-10-4559-2010)
- Meywerk J, Ramanathan V (1999) Observations of the spectral clear-sky aerosol forcing over the tropical Indian ocean. *Journal of Geophysical Research: Atmospheres*. doi:[10.1029/1999JD900502](https://doi.org/10.1029/1999JD900502)
- Michael M, Yadav A, Tripathi S, Kanawade V, Gaur A, Sadavarte P, Venkataraman C (2014) Simulation of trace gases and aerosols over the Indian domain: evaluation of the wrf-chem model. *Geosci Model Dev Discuss* 7(1):431–482
- Morrison H, Thompson G, Tatarskii V (2009) Impact of cloud microphysics on the development of trailing stratiform precipitation in a simulated squall line: Comparison of one- and two-moment schemes. *Mon Weather Rev* 137(3):991–1007. doi:[10.1175/2008MWR2556.1](https://doi.org/10.1175/2008MWR2556.1)
- Niranjan K, Sreekanth V, Madhavan B, Krishna Moorthy K (2007) Aerosol physical properties and radiative forcing at the outflow region from the indo-gangetic plains during typical clear and hazy periods of wintertime. *Geophys Res Lett* 34(19)
- Pai D, Sridhar L, Rajeevan M, Sreejith O, Satbhai N, Mukhopadhyay B (2014) Development of a new high spatial resolution (0.25 × 0.25) long period (1901–2010) daily gridded rainfall data set over India and its comparison with existing data sets over the region. *Mausam* pp p1–18
- Parashar D, Gadi R, Mandal T, Mitra A (2005) Carbonaceous aerosol emissions from India. *Atmos Environ* 39(40):7861–7871
- Pervez Y, Kushawaha S, Nair S, Pervez S (2016) Status of atmospheric carbonaceous matter in various locations of India. *Asian J Chem* 28(6):1261
- Prasad A, Singh R (2007) Changes in aerosol parameters during major dust storm events (2001–2005) over the indo-gangetic plains using aeronet and modis data. *Journal of Geophysical Research: Atmospheres* 112(D9)

- Ramachandran S, Cherian R (2008) Regional and seasonal variations in aerosol optical characteristics and their frequency distributions over India during 2001–2005. *Journal of Geophysical Research: Atmospheres* 113(D8)
- Ramanathan V, Carmichael G (2008) Global and regional climate changes due to black carbon. *Nat Geosci* 1(4):221–227
- Ramanathan V, Ramana M (2005) Persistent, widespread, and strongly absorbing haze over the himalayan foothills and the indo-gangetic plains. *Pure Appl Geophys* 162(8-9):1609–1626
- Ramanathan V, Crutzen P, Lelieveld J, Mitra A, Althausen D, Anderson J, Andreae M, Cantrell W, Cass G, Chung C, et al. (2001) IndiaN ocean experiment: An integrated analysis of the climate forcing and effects of the great indo-asian haze. *J Atmos Sci* 106(D22):28,371–28,398
- Ramanathan V, Chung C, Kim D, Bettge T, Buja L, Kiehl J, Washington WM, Fu Q, Sikka DR, Wild M (2005) Atmospheric brown clouds: impacts on South Asian climate and hydrological cycle. *Proc Natl Acad Sci USA* 102(15):5326–5333. doi:[10.1073/pnas.0500656102](https://doi.org/10.1073/pnas.0500656102)
- Randall D, Wood R, Bony S, Colman R, Fichet T, Fyfe J, Kattsov V, Pitman A, Shukla J, Srinivasan J, et al. (2007) Climate models and their evaluation. In: *Climate change 2007: The physical science basis. Contribution of Working Group I to the Fourth Assessment Report of the IPCC (FAR)*. Cambridge University Press, Cambridge, pp 589–662
- Randles C, Ramaswamy V (2008) Absorbing aerosols over asia: a geophysical fluid dynamics laboratory general circulation model sensitivity study of model response to aerosol optical depth and aerosol absorption. *Journal of Geophysical Research: Atmospheres* 113(D21)
- Remer L, Kaufman Y, Tanré D, Mattoo S, Chu D, Martins J, Li R, Ichoku C, Levy R, Kleidman R, Eck T, Vermote E, Holben B (2005) The MODIS aerosol algorithm, products, and validation. *J Atmos Sci* 62(4):947–973. doi:[10.1175/JAS3385.1](https://doi.org/10.1175/JAS3385.1)
- Safai P, Kewat S, Praveen P, Rao P, Momin G, Ali K, Devara P (2007) Seasonal variation of black carbon aerosols over a tropical urban city of pune, India. *Atmos Environ* 41(13):2699–2709
- Schell B, Ackermann I, Hass H (2001) Modeling the formation of secondary organic aerosol within a comprehensive air quality model system. *Journal of Geophysical Research: Atmospheres*. doi:[10.1029/2001JD000384](https://doi.org/10.1029/2001JD000384)
- Schultz M, Backman L, Balkanski Y, Bjoerndalsaeter S, Brand R, Burrows J, Dalsoeren S, de Vasconcelos M, Grodtmann B, Hauglustaine D (2007) Emission data sets and methodologies for estimating emissions, reanalysis of the tropospheric chemical composition over the past 40 years—a long-term global modeling study of tropospheric chemistry funded under the 5th eu framework programme, eu contract evk2-ct-2002-00170, work package 1, eur. comm., brussels
- Seethala C, Pandithurai G, Fast J, Polade S, Reddy M, Peckham S (2011) Evaluating wrf-chem multi-scale model in simulating aerosol radiative properties over the tropics—a case study over India. *Mapan* 26(4):269–284
- Shukla J (1998) Predictability in the midst of chaos: A scientific basis for climate forecasting. *Science* 282(5389):728–731
- Solmon F, Nair V, Mallet M (2015) Increasing arabian dust activity and the Indian summer monsoon. *Atmos Chem Phys* 15:8051–8064
- Srivastava A, Tripathi S, Dey S, Kanawade V, Tiwari S (2012) Inferring aerosol types over the indo-gangetic basin from ground based sunphotometer measurements. *Atmos Res* 109:64–75
- Stockwell W, Middleton P, Chang JS, Tang X (1990) The second generation regional acid deposition model chemical mechanism for regional air quality modeling. *J Geophys Res Atmos* 95(D10):16,343–16,367. doi:[10.1029/JD095iD10p16343](https://doi.org/10.1029/JD095iD10p16343)
- Twomey S (1977) The influence of pollution on the shortwave albedo of clouds. *Journal of the Atmospheric Sciences*. [http://journals.ametsoc.org/doi/abs/10.1175/1520-0469\(1977\)034](http://journals.ametsoc.org/doi/abs/10.1175/1520-0469(1977)034)
- Venkataraman C, Habib G, Kadamba D, Shrivastava M, Leon JF, Crouzille B, Boucher O, Streets DG (2006) Emissions from open biomass burning in india: Integrating the inventory approach with high-resolution moderate resolution imaging spectroradiometer (modis) active-fire and land cover data. *Glob Biogeochem Cycles* 20(2):n/a–n/a. doi:[10.1029/2005GB002547](https://doi.org/10.1029/2005GB002547), gB2013
- Vinoj V, Rasch P, Wang H, Yoon J, Ma P, Landu K, Singh B (2014) Short-term modulation of Indian summer monsoon rainfall by west asian dust. *Nat Geosci* 7(4):308–313
- Wang C, Kim D, Ekman A, Barth M (2009) Impact of anthropogenic aerosols on Indian summer monsoon. *Journal of Geophysical Research: Atmospheres*. doi:[10.1029/2009GL040114](https://doi.org/10.1029/2009GL040114)
- Wu L, Su H, Jiang J (2013) Regional simulation of aerosol impacts on precipitation during the east asian summer monsoon. *J Geophys Res Atmos* 118(12):6454–6467. doi:[10.1002/jgrd.50527](https://doi.org/10.1002/jgrd.50527)